Desalination and Water Treatment
www.deswater.com
doi: 10.5004/dwt.2020.26344

205 (2020) 189–197
November

In situ transport and electrodeposition of Ag(I) on stainless steel electrode across carrier mediated supported liquid membrane

Hanif-ur-Rehman, Anwar ul Haq Ali Shah, Adnan Khan, Nauman Ali*

Institute of Chemical Sciences, University of Peshawar, Pakistan, Tel. +92 91-9216652; Mob. +923322233010; email: nali75pk@uop.edu.pk (N. Ali), Mob. +923449796771; email: chem.ics.edu.pk@gmail.com (Hanif-ur-Rehman), Mob. +923459318002; email: anwarulhaqalishah@upesh.edu.pk (A. ul Haq Ali Shah), Mob. +923009890269; email: adnankhan@uop.edu.pk (A. Khan)

Received 26 December 2019; Accepted 14 July 2020

ABSTRACT

Ag(I) has been electrodeposited on a stainless steel electrode inserted in strip side solution across tri-*n*-dodecylamine-xylene base supported liquid membrane. The electrodeposition of Ag^+ was dependent on different variables like current density, tri-*n*-dodecylamine (TDDA) concentration in the liquid membrane, nitric acid (HNO_3) concentration in the feed solution, ammonia (NH_3) concentration in strip phase, stirring speed and source concentration. The optimum conditions for the electrodeposition of Ag^+ are 0.957 M TDDA in membrane phase, 1.0 M NH_3 in strip solution, 1.0 M HNO_3 in the feed solution, 6×10^{-1} mM Ag^+ in source and 900 rpm of stirring speed. The complex formation was confirmed through graphical elucidation whereas the number of moles of TDDA interacting with Ag^+ was one. The electrodeposition of Ag^+ on the stainless steel electrode was verified via inductively coupled plasma and Faraday laws. The recovery of the Ag^+ has been exceeded up to 99.40% from 98% coupling with three-electrode system. The stability of the membrane was the same as 120 h.

Keywords: TDDA; Electrodeposition; Silver; Three electrode system

1. Introduction

The demand for silver has amplified significantly recently due to utilization in the fields of purification, manufacturing of photographic film and medicine [1–6]. The silver is extracted from the main ores [3]. Silver is mainly extracted through mining via traditional ways since long ago. Therefore, the scientists have utilized various kinds of techniques to improve the efficiency of silver extraction such as solvent extraction, liquid-liquid powder extraction, adsorption, cloud point extraction, ionic liquid microextraction, bulk liquid membrane, emulsion liquid membrane, photocatalytic deposition, and solid-phase extraction [7–12]. The solvent extraction along with other conventional methods has the limitation in processing large scale processes due to cost-effectiveness and time-consuming requirements [13–16].

As time passed various new methods have been developed for improving the efficiency of the process. Electromembrane extraction was studied by the ab-initio method for various ions transportation through the supported liquid membrane (SLM) which forms a thin layer of hydrophobic organic solvent on the membrane phase [17–21]. It results in the impulse of an electric potential to produce the thrust for a higher extraction rate of various ions.

Over the past few decades, a lot of techniques were in use to extract silver from aqueous solutions but resulted either in low percent extraction or serious operating limitations like low loading and detection limits, low extraction rate and efficiency, carcinogenic and expensive nature, emulsification, and Poor sensitivity, etc. [20]. Extractants having P(S)SH functional groups were effective for silver extraction in a particular range of concentration but

* Corresponding author.

showed weak extraction in low concentration regions and no extraction was observed in high concentration regions. The unmodified calixarenes and carboxylate derivatives were used as extractants for silver and showed poor separation efficiency [22–24]. Simple ethers were modified to macrocyclic or giant polycyclic and crown ethers which enhanced the extraction efficiency from 80% to 94%, however, the recovery rate from the membrane interface to the stripping solution was only 81% [24–30]. Due to high expense and toxicity phosphines, oximes, and thiols are replaced with organic amines in the last decade. The percent recovery was exceeded from 94 to 97 by selecting macrocyclic chelating amines and reached 99 when Potassium cyanide coined a perfect match with the triethanolamine carrier. However, the three OH groups in triethanol ammine further increases the water miscibility which greatly affects the chemical and mechanical strength of the SLM. Recently the toxic cyanide strippers have substituted with more eco-friendly ammonia results almost the same percent recovery [31–33].

In the beginning, researchers have reported the transport and identification of Ag^+ ions across the SLM via electrode [32]. The present work is focused on the extraction of silver from feed to strip by coupling with electrodeposition application as ab-initio being employed in the SLM technique for the transport of silver ions. The optimized process was applied to the silver ore and plating waste which selectively deposited silver on the electrode. This method was employed because of the selectivity of SLM for the metal ion. It will create an up-thrust force for metal ions transportation through the membrane by chemical as well as electrical gradient which will control the current-voltage ratio. Hence, we are expected with a higher percentage of Ag^+ ions extraction through SLM in less time.

2. Theory

Electrodeposition of Ag^+ through tri-*n*-dodecylamine (TDDA) in xylene based SLM incorporated in microporous polymeric polypropylene film has been performed. Ag^+ transports from feed solution to membrane interface due to the uphill force of basic carrier. Being a strong ligand, NH_3 can easily dissociate the Ag^+ carrier complex.

In the equation, TDDA can be expressed as C. Basic TDDA at the source side of the membrane possibly protonates to CH^+ in acidic solution. The HNO_3 in the feed phase may propagate the silver nitrate reaction in the following way [28].

$$AgNO_{3aq} + nNO^-_{3aq} \rightleftharpoons [Ag(NO_3)_{n+1}]^{n-}_{aq} \quad (1)$$

where CH^+ and $[Ag(NO_3)_{n+1}]^{n-}$ interact at the source side of the membrane to form the complex as per the following equation:

$$nCH^+_{org} + \left[Ag\left(NO_3\right)_{n+1}\right]^{n-}_{aq} \rightleftharpoons \left(CH\right)_n \cdot Ag\left(NO_3\right)_{n+1\,org} \quad (2)$$

The subscripts org. and aq. illustrate the organic and aqueous phases, respectively. To signify the part of H^+ and NO^-_3, Eq. (2) may be modified as:

$$Ag^+_{aq} + (n+1)(NO_3)^-_{aq} + nC_{org} + nH^+_{aq} \rightleftharpoons (CH)_n \cdot Ag(NO_3)_{n+1org} \quad (3)$$

where Ag(I), H^+, and NO^-_3 exhibit co-ion transport mechanism which ultimately move towards the stripping phase. As per Eq. (3), the proposed complex pervades from source solution to liquid membrane interface which permeates to membrane stripping interface due to concentration and viscosity difference. $[Ag(NH_3)_2]^+$ is formed after dissociation of $(CH)_n \cdot Ag(NO_3)_{n+1org}$ at membrane stripping interface attributes the presence of $NH_{3(aq)}$ in the stripping phase [31]. The carrier C unloads which permeates back to the side of the membrane, ultimately Ag(I) extracted as electrodeposited from the feed phase into the stripping phase.

The equilibrium is constant for Eq. (3) can be given as:

$$K_{Ag} = \frac{\left[\left(CH\right)_n \cdot Ag\left(NO_3\right)_{n+1}\right]_{orgc}}{\left[Ag^+\right]_{aqu} \cdot \left[NO^-_3\right]^{n+1}_{aqu} \cdot \left[H^+\right]^n_{aqu} \cdot \left[C\right]^n_{orgc}} \quad (4)$$

The distribution coefficient of Ag(I), (λ_{Ag}), can be written as:

$$\lambda_{Ag} = \frac{\left[\left(CH\right)_n \cdot Ag\left(NO_3\right)_{n+1}\right]_{orgc}}{\left[Ag^+\right]_{aqu}} \quad (5)$$

Eq. (4) can be modified as:

$$K_{Ag} = \frac{\lambda_{Ag}}{\left[NO^-_3\right]^{n+1}_{aqu} \cdot \left[H^+\right]^n_{aqu} \cdot \left[C\right]^n_{orgc}} \quad (6)$$

By rearranging Eq. (6), it becomes as:

$$\lambda_{Ag} = K_{Ag} \cdot \left[NO^-_3\right]^{n+1}_{aqu} \cdot \left[H^+\right]^n_{aqu} \cdot \left[C\right]^n_{orgc} \quad (7)$$

The species enclosed in brackets show the activities which are involved in transport. The Ag^+ ion complex formation on the membrane interface is very fast for consideration also its dissociation. Thus, the transport of Ag(I) via SLM is considered to be the rate-determining step. Fick's law is given as:

$$J = \frac{\left(1/A\right)dN}{dt} \quad (8)$$

where N is used for the quantity of permeate and t represents the time of transport. The flux J is given as:

$$J = \frac{D\left(\lambda_f \cdot C_f - \lambda_s \cdot C_s\right)}{\ell} \quad (9)$$

In Eq. (9) λ describes the distribution coefficients of Ag(I), subscripts f and s represent feed and strip respectively. The C_f and C_s indicate the bulk feed and stripping concentrations of Ag(I), respectively.

Permeability coefficient *p*, the distribution coefficient and diffusion coefficient (*D*) are related by the equation as:

$$p = D\lambda \tag{10}$$

If $\lambda_f = \lambda_s$ then:

$$J = \frac{p\left(C_f - C_s\right)}{\ell} \tag{11}$$

As the back transport of Ag(I) from the stripping phase into the membrane phase is not possible, therefore, λ_s tends to zero and Eq. (9) alters to:

$$J = \frac{D \cdot \lambda_f \cdot C_f}{\ell} \tag{12}$$

where $\lambda_f = \lambda_{Ag}$ as given by Eq. (7), therefore,

$$J = \frac{D \cdot K_{Ag} \cdot \left[NO_3^-\right]_{aqu}^{n+1} \cdot \left[H^+\right]_{aqu}^{n} \cdot \left[C\right]_{org}^{n} \cdot C_f}{\ell} \tag{13}$$

$$\log J\eta = \frac{\begin{array}{c}\text{constant} + (n+1)\log\left[\left(NO_3\right)^{n-}\right]_{aqu} + \\ n\log\left[H^+\right]_{aqu} + n\log\left[C\right]_{orgc} + \log C_f\end{array}}{\ell} \tag{14}$$

Eq. (14) can be used to find the composition of the complex, by varying only one parameter while keeping the others constant. The number of H^+ and C can be calculated in different ways; by keeping $[NO_3^-]$, [C], *l* and C_f constant and plot log*J*h vs. log $[H^+]$, the slope of the graph will illustrate the number of H^+ and another way is to keep $[NO_3^-]$, $[H^+]$, *l* and C_f constant, the slope of log*J*h against log[C] will give a number of molecules of tri-*n*-dodecylamine contributing to the complex formation. Electrodeposition has been accessed from the following equation. The amount of silver metal deposited (*W*) on the stainless steel plate was calculated by the weight difference method and justified using the Faraday's relation. Where *W* is the weight of the deposited metal in grams, *I* is current in ampere units, *e* is the charge of electron and *F* is a Faraday constant.

$$W = \frac{Ite}{F} \tag{15}$$

3. Experimental setup

3.1. Chemicals and reagents

The silver nitrate (Merck 99.8%, UK) in nitric acid (HNO_3, Merck ≥ 65%) was utilized as a source solution. Tri-*n*-dodecylamine (TDDA, Merck ≥ 95%) was incorporated in pores of polypropylene flat sheet as a liquid membrane in xylene (Sigma 98.5%, Germany) as a thinner to prepare SLM with various concentrations. Ammonia (NH_3, Merck ≥ 98.98%) was used as a strippant. Deionized water was used throughout the research venture. The whole listed chemicals were of analytical grade.

3.2. Apparatus and instruments

Inductively coupled plasma spectrometer, Perkin Elmer model Avio 500 (USA) was used to find out the unknown concentration of metal ions in feed and strip solutions. Feed and strip pH were measured periodically using pH meter. Carrier-xylene viscosity was measured by Brookfield LDV-III viscometer (China). All the glassware was made of borax glass of premium quality.

3.3. Membrane support

Polymers are versatile materials and they find applications in various scientific fields [34–38]. Polypropylene membrane, Celgard 2400 (China) was used as membrane support. The thickness of the PP sheet was 25 μm while the porosity was 45%. The PP sheet was soaked in a known concentration of TDDA in xylene overnight.

3.4. Permeation unit

The cell is composed of two 250 cm^3 rectangular compartments having a circular opening of 20 cm^2 in the middle of one side of acrylic sheets. An adjustable membrane jacket with a stiff inert rubber was placed on each side and clamped between two compartments to stop leakage. The electric motors with the range of 100–1,500 rpm were placed on the top of both cells having porthole also for pH electrode and sampling.

3.5. Preparation of electrode

The stainless steel electrodes were prepared for electrodeposition of Ag^+ ions. The electrodes were cleaned with dilute hydrochloric acid to remove the impurities. A stainless steel electrode of the surface area of 1.0 cm^2 was dipped in solution for electrodeposition.

3.6. Extraction and electrodeposition study of silver ions

The Ag ions were extracted using the TDDA-xylene polypropylene SLM system from the simulated silver wastewater and ore. Different concentrations of silver solutions ranging from 100 to 600 ppm were prepared. In the case of concentration of acid optimization the feed solution was prepared by an appropriate amount of acid addition before diluting to required 100 to 600 ppm range. The optimization of the reaction was performed by altering the parameters such as the concentration of metal ions in feed, the concentration of acid in feed, the concentration of carrier and concentration of ammonia in strip solution.

Electrochemical reduction (electrometallurgy) of Ag^+ was carried out in a prototype, fabricated into two compartments of acrylic sheet. A SLM was sandwiched in between the two compartments, impregnated with organic liquid for the transport of these ions. Electrodeposition occurred at the cathode on the strip side of the cell. A three-electrode system was installed in a single strip side top. Stainless steel

rods with an effective area of one cm^2, strips were used as working and counter electrodes while $Ag/AgCl_2$ reference electrode was prepared indigenously in a reported shape. The stirring speed of agitators was adjusted through the DC transformer and regulator. During the permeation and electrodeposition study, the speed of the stirrer was sensed using local rpm sensors. Ammeter was connected between working and counter electrode in series while voltmeter was connected with the reference electrode in parallel. The negative terminal of the 12-V dry battery was connected with a working stainless-steel electrode and positive terminal with the counter electrode to act as cathode and anode respectively. The whole setup is shown in Fig. 1.

The amount of metal ions deposited, rate of deposition and all other parameters were studied from the relation of Faraday's and Ohm laws theoretically as shown in Eq. (15) at optimum conditions. Where W is the weight in grams of reduced silver ions that deposited on an electrode in the presence of current I, in amperes and time t, in seconds. The empirical value of silver deposition on the electrode was calculated from the electrode weight difference method.

4. Results and discussion

4.1. Effect of carrier (TDDA) concentration on electrodeposition

This research reveals the impact of TDDA concentration on the electrodeposition of Ag^+, employing a series of TDDA concentration from 0.191 to 1.341 M. Besides the constant potential, Ag^+ concentration was retained at 6.0×10^{-1} mM in 1.0 M of HNO_3 in source and concentration of NH_3 was fixed at 1.0 M in strip solution.

Fig. 2 represents the electrodeposition of Ag^+ on the surface of the stainless steel electrode for variation in TDDA concentration in the membrane phase. The graph illustrates that the electrodeposition of Ag^+ increases from 0.0176 to 0.2830 g as the concentration of TDDA exceeds from 0.191 to 0.957 M. The electrodeposition of Ag^+ diminishes above 0.957 M of TDDA. As the concentration of carrier increases, the stripping of Ag^+ from feed to strip phase also increases which facilitates the electrodeposition through the availability of the excess amount of Ag^+ ions.

An abrupt fall in transport and electrodeposition of Ag^+ above 0.957 M can be justified by the enhanced viscosity of TDDA in the membrane phase. The increase of TDDA concentration in the membrane phase in xylene the viscosity also increases which retards the transport Ag^+ ultimately less electrodeposition of Ag^+. The 99.40% transported Ag^+ has been deposited on the stainless-steel electrode at TDDA concentration of 0.957 M. Subsequently, 0.957 M was taken as the optimal concentration for transport and electrodeposition of Ag^+ and the same concentration was used to optimize the other parameters of electrodeposition. The experimental deposited mass of Ag^+ is less than a theoretical value by a factor of 0.006. The difference in theoretical and experimental values is 0.6% which might be attributed to the experimental errors.

4.2. Effect of HNO_3 concentration on transport and electrodeposition

HNO_3 provides both proton and NO_3^- for producing CH^+ and $[Ag(NO_3)_{n+1}]^{n-}$ type species respectively and performs an essential function in the transportation of Ag^+ ions. HNO_3 concentration was altered from 0.4 to 1.5 M during the whole span of the experiment while the concentration of carrier in the liquid membrane and NH_3 on the strip side was kept constant at 0.957 and 1.0 M, respectively.

Fig. 3 evinces that deposition of Ag^+ enhances from 0.025 to 0.283 g with elevation in the concentration of HNO_3 from 0.4–1.0 M to a maximum value at 1.0 M. This is because of the co-ion transport mechanism of Ag^+ across the membrane to stripping phase and increased current density (CD, $i = I/S$). Above 1.0 M of HNO_3 results in a decline in the deposition of Ag^+. The H^+ ions in excess might disproportionate the permeation of Ag^+ through a membrane which led to decrease electrodeposition.

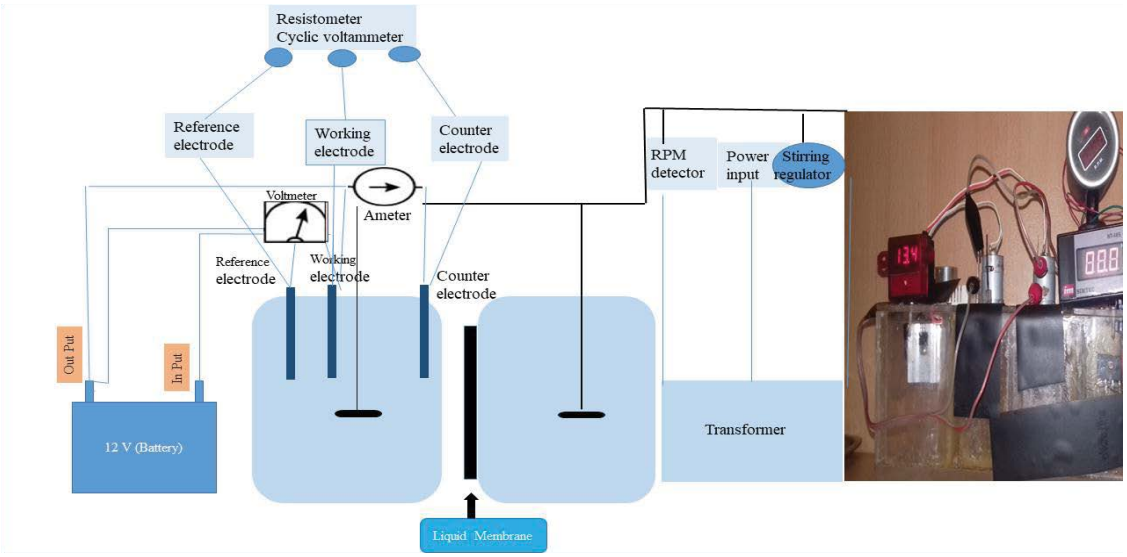

Fig. 1. Permeation and electrodeposition unit.

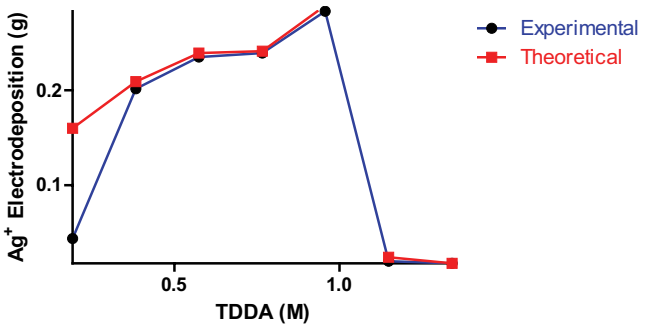

Fig. 2. Electrodeposition variation at various concentrations of TDDA in the membrane.

4.3. Impact of stripping phase concentration (NH_3) on permeation and current density

NH_3 works as a stripping agent in the stripping phase of the permeation unit. Various concentrations run from 0.4 M to 1.5 M of NH_3 were used while the concentration of HNO_3 was fixed at 1.0 M and concentration of TDDA at 0.957 M in the liquid membrane. Previous research work demonstrates that without the strippant the transport of Ag^+ was not possible even if the cell runs for 8 h [33]. Therefore, the NH_3 strives the Ag^+ into the stripping phase by dissociating the Ag-TDDA complex. It is seen from Fig. 4 that with an increase in NH_3 concentration from 0.4–1.0 M, the permeation of Ag^+ and current density hits the maximum exactly at 1.0 M. The impact of $NH_{3(aq)}$ on the transport and deposition of Ag^+ can be illustrated by the two obvious reasons. Firstly OH^- ions of NH_3 may interact with the H^+ of the complex $((CH)_n \cdot Ag(NO_3)_{n+1})$ which results in the dissociation of the complex as shown.

$$CH_n \cdot (AgNO_3)_{n+1} + OH^- \rightarrow nC + [(AgNO_3)_{n+1}]^{n-} + H_2O \quad (16)$$

Also, the free NH_3 molecules can attack the silver in $[(AgNO_3)_{n+1}]^{n-}$ and result in the formation of diamine soluble complex ion [32].

$$[(AgNO_3)_{n+1}]^{n-} + 2NH_3 \rightarrow Ag(NH_3)_2^+ + (n+1)NO_3^- \quad (17)$$

Due to these two reasons, more Ag^+ ions enter into the stripping medium and hence enhance the current density which occurs because of an uninterrupted supply of Ag^+ ions from strip solution to the electrode. However, the sudden fall in current density after 1.0 M of NH_3 may be due to the extraction of H^+ ions from the carrier and reduces the capability of the carrier to extract Ag^+ ions simultaneously.

4.4. Variation in Ag^+ concentration in source solution

The concentrations variation of Ag^+ ions from 2×10^{-1} mM to 10×10^{-1} mM were utilized to probe the impact of Ag^+ concentration on flux and electrodeposition. The concentration of HNO_3 in the feed phase was kept constant at 1.0 M, NH_3 in the strip phase at 1.0 M, and tri-*n*-dodecylamine in the membrane phase at 0.957 M. The flux of Ag^+ increases with the increase in the concentration of Ag^+ as

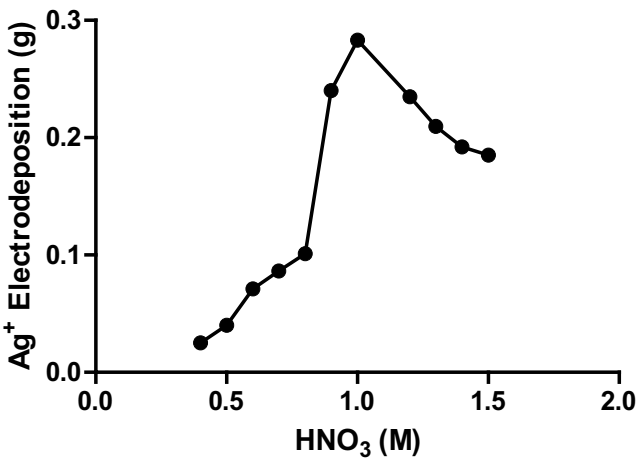

Fig. 3. Electrodeposition at various concentrations of HNO_3 in source solution.

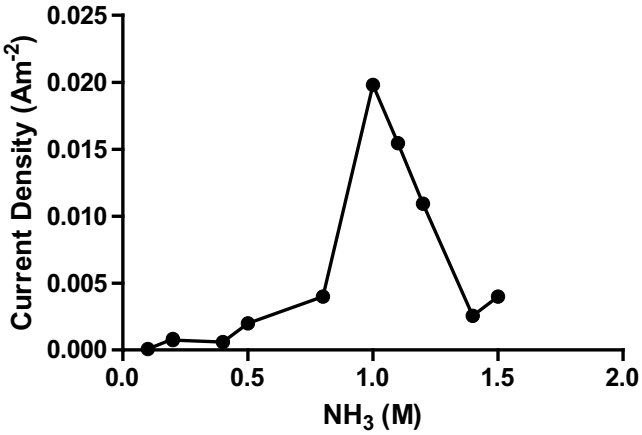

Fig. 4. Current density variation at various concentrations of NH_3 in strip solution.

verified in previous work [31]. Electrodeposition of Ag^+ occurs according to the same pattern with the exception at a high concentration of Ag^+. The deposition of silver on the stainless steel electrode increases from 0.0015 to 0.283 g as the concentration of Ag^+ increases from 2×10^{-1} mM to 6×10^{-1} mM and reaches a maximum at the concentration of Ag^+ in feed solution as shown in Fig. 5. Nevertheless, the deposition decreases beyond 6×10^{-1} mM of Ag^+ in feed solution contrary to flux across the membrane. The anomalous behavior is probably due to diffused double layer formation or shear local concentration of Ag^+ near the electrode interface.

4.5. Effect of string speed on electrodeposition

The speed of agitator enhances the electrodeposition process in respect of time and quantity. Different rpm of the range 100 to 1,500 was used to observe the effect of string speed of electrical motors on the deposition of Ag^+ on the electrode. Various speeds of agitator in rpm range from 100–1,500 rpm were investigated on the electrodeposition

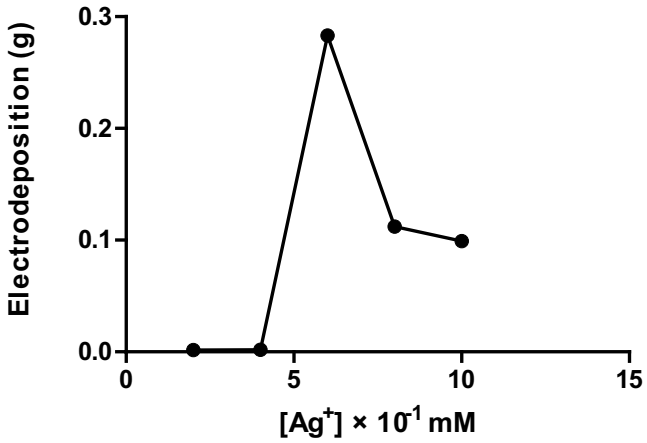

Fig. 5. Effect of Ag^+ concentration in feed solution on electrodeposition.

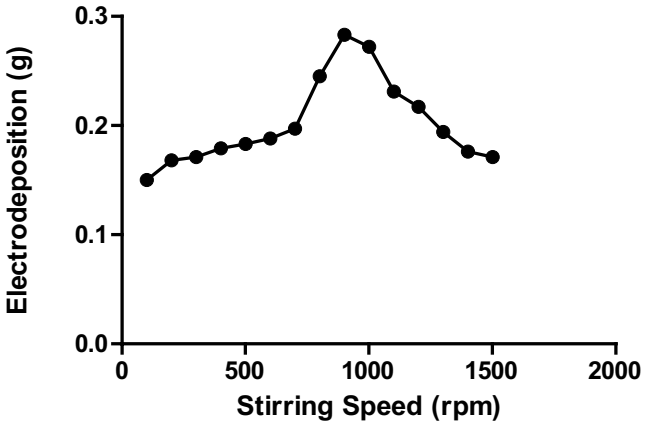

Fig. 6. Effect of stirring speed (rpm) on electrodeposition.

of Ag^+ on the stainless steel electrode. It was evident from Fig. 6 that as the stirring speed increases led to the increase in the deposition process at 900 rpm. Above 900 rpm electrodeposition decreases because at high rpm the diffusional layers break on feed interface and carrier drains out from the pores of the membrane which reduces the interaction of Ag^+ with carrier and finally the transport and deposition of Ag^+ on stainless steel electrode.

4.6. Effect of carrier concentration on flux

Eq. (13) indicates that as the TDDA concentration increases in the liquid membrane, the flux of Ag^+ also increases. This behavior is due to the interaction of more numbers of the carrier with H^+ to form CH^+, which in turn react with anions ($[Ag(NO_3)_{n+1}]^{n-}$), and increases the formation of the complex. Fig. 7 implies that the maximum increase in the flux was observed at 0.957 M of TDDA after that continuous decrease in the flux of Ag^+ was observed due to the increase in the viscosity of the liquid membrane phase. An increase in TDDA concentration in xylene is directly related, to the viscosity of the liquid membrane. Stokes–Einstein equation [14] gives the relation between the diffusion coefficient of the solute and viscosity of the liquid membrane as follows:

$$D = \frac{kT}{6\mu\pi r} \tag{18}$$

According to Eq. (18) the flux of Ag^+ is inversely proportional to the viscosity η of the carrier in the liquid membrane phase.

4.7. Stoichiometry of SLM

The number of TDDA molecules in complex formation has been determined from Fig. 8a. A graph log[TDDA] vs. log*J*η gives the slope of 1.0009 which indicates that only one molecule of TDDA is responsible for complexation as shown in Fig. 8a. In the same way, a graph is plotted between log[HNO_3] vs. log*J*η as shown in Fig. 8b. The number of H^+ ions furnished by HNO_3 for protonation of TDDA is

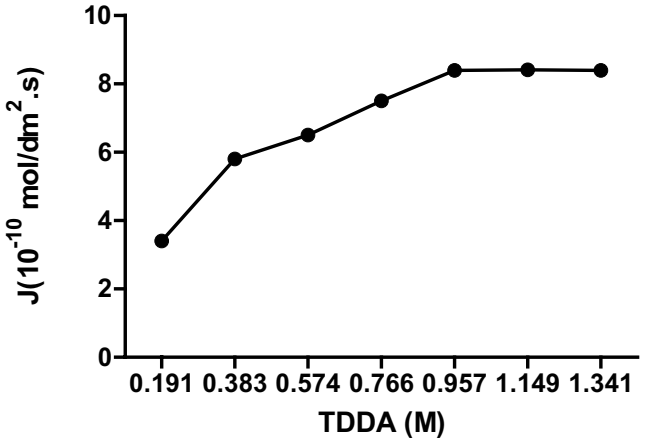

Fig. 7. Effect of TDDA concentration on the flux of Ag^+ ion.

determined from the slope of Fig. 8b. It comes out to be 1.055 which shows that approximately one proton is responsible for protonation of TDDA by HNO_3. In case of OH^- ligand only one silver ion is stripped off to the receiving phase while in case of free NH_3 the ratio of metal to the ligand is 1:2 which shows that two ligands are coordinating with one silver ion [39]. The reaction mechanism of the whole process is given:

$$AgNO_3 + HNO_3 \rightleftharpoons [Ag(NO_3)_2]^- + H^+ \tag{19}$$

$$R_3N + H^+ \rightleftharpoons R_3NH^+ \tag{20}$$

$$[Ag(NO_3)_2]^- + R_3NH^+ \rightleftharpoons (R_3NH^+ \cdot Ag(NO_3)_2) \tag{21}$$

$$n(R_3NH^+ \cdot Ag(NO_3)_2) + nNH_3 \rightleftharpoons n[Ag(NH_3)_2]^+ + nNO_3^- + nR_3N \tag{22}$$

where nR_3N shows η number of moles of TDDA molecule.

5. Stability of SLM

Despite emerging technology, SLM has several shortcomings like blockage of membrane pores, carrier or

solvent solubility in the aqueous phase, osmotic pressure and wetness of membrane orifices [40].

A membrane was soaked overnight in 0.957 M TDDA-xylene and applied for 5 experiments with 4 h each after a time interval of 24 h. It is found that the membrane flux and electrodeposition were uniform in each run up to 120 h as shown in Fig. 9. The recovery of Ag^+ was 99.40% when coupled with the three-electrode system.

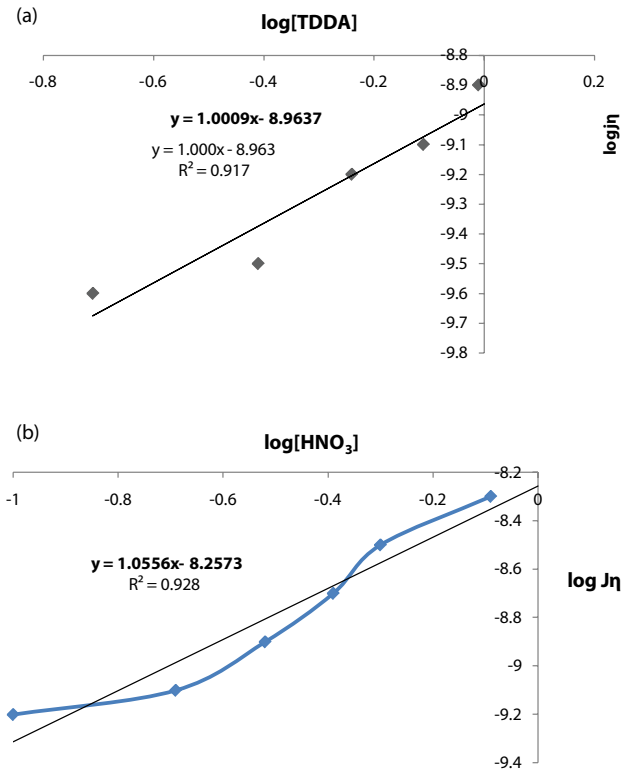

Fig. 8. (a) Plot log[TDDA] vs. log $J\eta$ and (b) plot log[HNO_3] vs. log $J\eta$.

6. Electrodeposition of silver from ore and silver plating

Silver has been recovered and identified by previous researchers but not deposited on the electrode [41,42]. Therefore, the TDDA-SLM system was coupled with a three-electrode system to create a potential gradient and enhanced up-thrust force for maximum removal of Ag^+ from silver ores and silver plating waste. The optimized conditions for deposition of Ag^+ were: 0.957 M of TDDA in the membrane, 6×10^{-1} mM of Ag^+ and 1.0 M of HNO_3 in source solution, and 1.0 M of NH_3 in strip phase. Table 1 explores that 99.40 % of Ag^+ has electrodeposited on stainless steel electrode having an active strip area of 1 cm^2 for deposition of Ag^+ ions from both silver ores and silver plating waste. The reproducibility results of the electrodeposition of Ag^+ showed that this technique is selective as well as efficient.

7. Conclusions

- The recovery of Ag^+ has improved by introducing three electrodes SLM systems from 98% to 99.40%.
- The stainless steel electrode showed ion-selective behavior towards Ag^+ ions.
- The optimum conditions for this three-electrode coupled with the SLM system are 1.0 M of HNO_3 in the feed

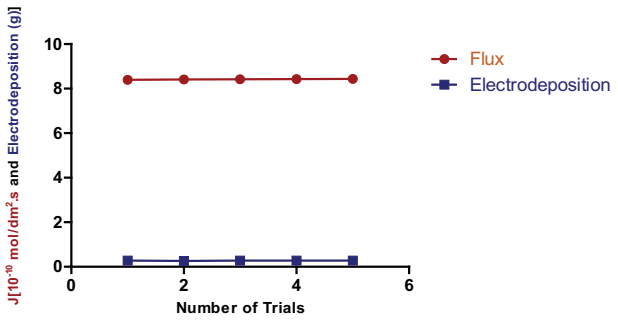

Fig. 9. Stability of SLM, number of trails vs. flux and electrodeposition of silver.

Table 1
Percent electrodeposition of silver in the presence of interfering metal ions

	Silver ore waste		Silver-plating waste		Silver ore and silver-plating waste
	Source concentration (BE)[a]	Source concentration (AE)[b]	Source concentration (BE)[a]	Source concentration (AE)[b]	Percent mean electrodeposition
Metal ions	BE (mg/L)	AE (mg/L)	BE (mg/L)	AE (mg/L)	(%)
Ag^+	300 ± 0.03	1.77 ± 0.008	300 ± 0.005	1.79 ± 0.09	99.40
Ni	Nil	Nil	9.5 ± 0.013	9.2 ± 0.008	0.03
Hg	Nil	Nil	Nil	Nil	Nil
Cu	2.8 ± 0.007	2.5 ± 0.005	3.0 ± 0.03	2.9 ± 0.05	0.07
Fe	2.9 ± 0.009	2.7 ± 0.01	Nil	Nil	0.06
Sb	3.30 ± 0.50	3.28 ± 0.05	Nil	Nil	0.006

[a]Before electrodeposition;
[b]After electrodeposition.

phase, 0.957 M of TDDA in the membrane and 1.0 M of NH_3 in the stripping phase.
- The SLM three-electrode system was observed to be stable for 120 h.

This research did not receive any specific grant from funding agencies in the public, commercial or not-for-profit sectors.

References

[1] Silver in Water Purification, The Silver Institute. Available at: https://www.silverinstitute.org/silver-water-purification/ (accessed June 22, 2019)
[2] Environmental Impact of Silver Nanoparticles, Wikipedia, 2018, Available at: https://en.wikipedia.org/w/index.php?title=Environmental_impact_of_silver_nanoparticles&oldid=845979434 (accessed June 22, 2019)
[3] S.J. Lee, D.N. Heo, M. Heo, M.H. Noh, D. Lee, S.A. Park, J.-H. Moon, I.K. Kwon, Most simple preparation of an inkjet printing of silver nanoparticles on fibrous membrane for water purification: technological and commercial application, J. Ind. Eng. Chem., 46 (2017) 273–278.
[4] D.J. Barillo, D.E. Marx, Silver in medicine: a brief history BC 335 to present, Burns, 40 (2014) S3–S8.
[5] J. Goel, K. Kadirvelu, C. Rajagopal, Mercury(II) removal from water by coconut shell based activated carbon: batch and column studies, Environ. Technol., 25 (2004) 141–153.
[6] N. Ali, M. Ismail, A. Khan, H. Khan, S. Haider, T. Kamal, Spectrophotometric methods for the determination of urea in real samples using silver nanoparticles by standard addition and 2nd order derivative methods, Spectrochim. Acta, Part A, 189 (2018) 110–115.
[7] T. Kamal, N. Ali, A.A. Naseem, S.B. Khan, A.M. Asiri, Polymer nanocomposite membranes for antifouling nanofiltration, Recent Pat. Nanotechnol., 10 (2016) 189–201.
[8] F. Wahid, I.U. Mohammadzai, A. Khan, Z. Shah, W. Hassan, N. Ali, Removal of toxic metals with activated carbon prepared from *Salvadora persica*, Arabian J. Chem., 10 (2017) S2205–S2212.
[9] A. Khan, S. Begum, N. Ali, S. Khan, S. Hussain, M.D.P.T. Sotomayor, Preparation of crosslinked chitosan magnetic membrane for cations sorption from aqueous solution, Water Sci. Technol., 75 (2017) 2034–2046.
[10] N. Ali, A. Zada, M. Zahid, A. Ismail, M. Rafiq, A. Riaz, A. Khan, Enhanced photodegradation of methylene blue with alkaline and transition-metal ferrite nanophotocatalysts under direct sun light irradiation, J. Chin. Chem. Soc., 66 (2019) 402–408.
[11] X.H. Lu, Q.X. Chen, D. Zhao, J.J. Zhu, J.B. Ji, Silver-based ionic liquid as separation media: supported liquid membrane for facilitated methyl linolenate transport, J. Membr. Sci., 585 (2019) 218–229.
[12] N. Ali, S. Azeem, A. Khan, H. Khan, T. Kamal, A.M. Asiri, Experimental studies on removal of arsenites from industrial effluents using tridodecylamine supported liquid membrane, Environ. Sci. Pollut. Res., 27 (2020) 11932–11943.
[13] S. Pedersen-Bjergaard, K.E. Rasmussen, Electrokinetic migration across artificial liquid membranes: new concept for rapid sample preparation of biological fluids, J. Chromatogr. A, 1109 (2006) 183–190.
[14] R. Nawaz, K. Ali, M. Arshad, Recovery of mercury using a trioctylphosphine oxide-based supported liquid membrane system, Environ. Eng. Sci., 32 (2015) 948–959.
[15] R. Nawaz, K. Ali, M. Khan, Extraction of copper from wastewater through supported liquid membrane using tri-ethanolamine as a carrier, Desal. Water Treat., 57 (2016) 21827–21841.
[16] R. Nawaz, K. Ali, N. Ali, A. Khaliq, Removal of chromium(VI) from industrial effluents through supported liquid membrane using trioctylphosphine oxide as a carrier, J. Braz. Chem. Soc., 27 (2016) 209–220.
[17] S. Pedersen-Bjergaard, C. Huang, A. Gjelstad, Electromembrane extraction–recent trends and where to go, J. Pharm. Anal., 7 (2017) 141–147.
[18] S. Pedersen-Bjergaard, Electromembrane extraction—looking into the future, Anal. Bioanal. Chem., 411 (2019) 1687–1693.
[19] C.-S. Yeh, P.-S. Cheng, S.Y. Chang, Solvent-free electromembrane extraction: a new concept in electro-driven extraction, Talanta, 199 (2019) 296–302.
[20] M.A. Barakat, New trends in removing heavy metals from industrial wastewater, Arabian J. Chem., 4 (2011) 361–377.
[21] N. Ali, N. Naz, Z. Shah, A. ul Haq Ali Shah, A. Khan, R. Nawaz, Selective transportation of molybdenum from model and ore through poly inclusion membrane, Bull. Chem. Soc. Ethiop., 34 (2020) 93–104.
[22] M.S. Alam, K. Inoue, K. Yoshizuka, Y. Dong, P. Zhang, Solvent extraction of silver from chloride media with some commercial sulfur-containing extractants, Hydrometallurgy, 44 (1997) 245–254.
[23] K. Ohto, E. Murakami, T. Shinohara, K. Shiratsuchi, K. Inoue, M. Iwasaki, Selective extraction of silver(I) over palladium(II) with ketonic derivatives of calixarenes from highly concentrated nitric acid, Anal. Chim. Acta, 341 (1997) 275–283.
[24] M. Oue, K. Kimura, T. Shono, Liquid-liquid extraction of silver ion with benzothiacrown ether derivatives, Anal. Chim. Acta, 194 (1987) 293–298.
[25] M. Shamsipur, S.Y. Kazemi, G. Azimi, S.S. Madaeni, V. Lippolis, A. Garau, F. Isaia, Selective transport of silver ion through a supported liquid membrane using some mixed aza-thioether crowns containing a 1,10-phenanthroline sub-unit as specific ion carriers, J. Membr. Sci., 215 (2003) 87–93.
[26] S. Altin, Y. Yildirim, A. Altin, Transport of silver ions through a flat-sheet supported liquid membrane, Hydrometallurgy, 103 (2010) 144–149.
[27] O. Arous, H. Kerdjoudj, P. Seta, Comparison of carrier-facilitated silver(I) and copper(II) ions transport mechanisms in a supported liquid membrane and in a plasticized cellulose triacetate membrane, J. Membr. Sci., 241 (2004) 177–185.
[28] S.K. Ashok Kumar, Shipra, Manjusha, Dual behavior of thiuram sulfide: highly selective transport and ion-selective electrode for Ag(I) ions under two different conditions, J. Membr. Sci., 350 (2010) 161–171.
[29] B. Tang, G.J. Yu, J.Z. Fang, T.H. Shi, Recovery of high-purity silver directly from dilute effluents by an emulsion liquid membrane-crystallization process, J. Hazard. Mater., 177 (2010) 377–383.
[30] M. Ramos-Payán, R. Fernández-Torres, J.L. Pérez-Bernal, M. Callejón-Mochón, M.Á. Bello-López, A novel approach for electromembrane extraction based on the use of silver nanometallic-decorated hollow fibers, Anal. Chim. Acta, 849 (2014) 7–11.
[31] A.A. Amiri, A. Safavi, A.R. Hasaninejad, H. Shrghi, M. Shamsipur, Highly selective transport of silver ion through a supported liquid membrane using calix[4]pyrroles as suitable ion carriers, J. Membr. Sci., 325 (2008) 295–300.
[32] M.A. Chaudry, N. Bukhari, M. Mazhar, Coupled transport of Ag(I) ions through triethanolamine–cyclohexanone-based supported liquid membranes, J. Membr. Sci., 320 (2008) 93–100.
[33] S. ur Rehman, G. Akhtar, M.A. Chaudry, K. Ali, N. Ullah, Transport of Ag^+ through tri-*n*-dodecylamine supported liquid membranes, J. Membr. Sci., 389 (2012) 287–293.
[34] T. Kamal, I. Ahmad, S.B. Khan, A.M. Asiri, Agar hydrogel supported metal nanoparticles catalyst for pollutants degradation in water, Desal. Water Treat., 136 (2018) 290–298.
[35] T. Kamal, M. Ul-Islam, S.B. Khan, A.M. Asiri, Adsorption and photocatalyst assisted dye removal and bactericidal performance of ZnO/chitosan coating layer, Int. J. Biol. Macromol., 81 (2015) 584–590.
[36] F. Ali, S.B. Khan, T. Kamal, Y. Anwar, K.A. Alamry, A.M. Asiri, Anti-bacterial chitosan/zinc phthalocyanine fibers supported metallic and bimetallic nanoparticles for the removal of organic pollutants, Carbohydr. Polym., 173 (2017) 676–689.

[37] N. Ali, Awais, T. Kamal, M. Ul-Islam, A. Khan, S.J. Shah, A. Zada, Chitosan-coated cotton cloth supported copper nanoparticles for toxic dye reduction, Int. J. Biol. Macromol., 111 (2018) 832–838.
[38] T. Kamal, S.B. Khan, A.M. Asiri, Synthesis of zero-valent Cu nanoparticles in the chitosan coating layer on cellulose microfibers: evaluation of azo dyes catalytic reduction, Cellulose, 23 (2016) 1911–1923.
[39] G. Svehla, B. Sivasankar, Vogel's Qualitative Inorganic Analysis, 7th ed., Pearson Education, India, 2008.
[40] H. Ur Rehman, G. Akhtar, H. Ur Rashid, N. Ali, I. Ahmad, S. Ur Rehman, K. Khan, M. Arshad, Transport of Zn(II) by TDDA-polypropylene supported liquid membranes and recovery from waste discharge liquor of galvanizing plant of Zn(II), J. Chem., 2017 (2017) 1–9, https://doi.org/10.1155/2017/7569354.
[41] N. Othman, K.H. Chan, M. Goto, H. Mat, Emulsion liquid membrane extraction of silver from photographic waste using CYANEX 302 as the mobile carrier, Solvent Extr. Res. Dev., 13 (2006) 191–202.
[42] N. Othman, H. Mat, M. Goto, Selective extraction of silver from liquid photographic waste, Solvent Extr. Res. Dev., 12 (2005) 27–34.